Quantum Chemistry and Computational Kinetics of the Reaction between OH Radicals and Formaldehyde Adsorbed on Small Silica Aerosol Models

ARTICLE *in* THE JOURNAL OF PHYSICAL CHEMISTRY C · MARCH 2008

Impact Factor: 4.77 · DOI: 10.1021/jp077557m

4 AUTHORS, INCLUDING:

Cristina Iuga
Metropolitan Autonomous University
43 PUBLICATIONS **342** CITATIONS
SEE PROFILE

Alfonso Hernandez-Laguna
Instituto Andaluz de Ciencias de la Tierra
101 PUBLICATIONS **939** CITATIONS
SEE PROFILE

Claro Ignacio Sainz-Díaz
Instituto Andaluz de Ciencias de la Tierra
99 PUBLICATIONS **1,210** CITATIONS
SEE PROFILE

Quantum Chemistry and Computational Kinetics of the Reaction between OH Radicals and Formaldehyde Adsorbed on Small Silica Aerosol Models

Cristina Iuga,[†] Annik Vivier-Bunge,[†] Alfonso Hernández-Laguna,[‡] and C. Ignacio Sainz-Díaz*[,§]

Departamento de Química, Universidad Autónoma Metropolitana, Iztapalapa, México, D.F., Mexico, Estación Experimental del Zaidín, CSIC, C/ Prof. Albareda 1, 18008 Granada, Spain, and Laboratorio de Estudios Cristalográficos, IACT, CSIC-Universidad de Granada, Spain

Received: September 19, 2007; In Final Form: December 5, 2007

Heterogeneous reactions of atmospheric volatile organic compounds (VOCs) on aerosol particles may play an important role in atmospheric chemistry. Clay particles are present in mineral dust in atmospheric aerosols, and radical reactions are thought to be heterogeneously catalyzed on them. However, the kinetics and mechanisms of adsorption and reaction of atmospheric VOCs on aerosol surfaces are not well understood. In this work, quantum chemical methods are used to study the reaction of OH radicals with formaldehyde adsorbed on small $(SiO_4)_n$ cluster models, with $n = 1$ to 6. We show that surface adsorbed formaldehyde can react in the presence of gas-phase OH radicals to yield surface-bound formyl radicals and water. Significant exothermic adsorption energies are found, supporting the notion that silicate surfaces are good quenchers of VOCs. With the models employed, the reaction appears to be less favored on the silicate surfaces than in the gas phase. The effect of the model surface on the reaction mechanism is analyzed.

Introduction

A major natural component of atmospheric aerosol is mineral dust, which enters the atmosphere from dust storms in arid and semiarid regions. About 33% of the earth's land surface is arid, and it represents a potential source region for this atmospheric mineral aerosol.[1] The latter is a general expression for fine particles of crustal origin that are generated by wind erosion, and which consist mostly of silica and silicate minerals. Particles smaller than 10 μm have week-long atmospheric lifetimes,[2] and they may be transported over thousands of kilometers. The transatlantic transport of Saharan dust to North America is a well-studied phenomenon where silicate particles have been found in aerosols (see reviews [2,34] and recent articles[5−7]).

The chemical and mineralogical composition of mineral aerosols is complex.[8] Globally, the most important minerals of the clay fraction (<2 μm) transported in dust storms are phyllosilicates, mainly illite, kaolinite, chlorite, and smectite,[9] whereas coarser particles mainly consist of quartz, feldspars, and carbonates.[10] Dust aerosols in the lower stratosphere consist almost entirely of clay particles.[11]

Quartz, feldspars and phyllosilicates are mainly formed by basic units of SiO_4 with substitutions and different arrangements. For instance, phyllosilicates consist of sheets of SiO_4 tetrahedrons linked to a sheet of Al hydroxide octahedrons. Substitutions in any of the sheets give rise to a variety of minerals. They have large specific surfaces and catalytic properties. Therefore, their presence in aerosols can be expected to play an important role in the heterogeneous chemistry of the troposphere.

The potentially reactive surface of mineral aerosols may be a significant sink for many volatile organic compounds in the atmosphere, and consequently it could influence the global photooxidant budget. Laboratory studies, together with field observations and modeling calculations, have clearly demonstrated the importance of heterogeneous processes in the atmosphere. The subject has recently been reviewed by Usher et al.[12] Some authors have tried to quantify the effect of dust on tropospheric chemistry. Dentener et al.[13] calculated that ozone concentration would decrease because O_3 production decreased (N_2O_5 and HO_2 were taken up on dust) and because the O_3 molecules were themselves taken up on dust. In addition, results from this study suggest that a large fraction of gas-phase nitric acid may be neutralized by mineral aerosol. Bian and Zender[14] quantified the effect of dust on tropospheric chemistry due to photolysis and heterogeneous update. They found that, on a global average, O_3 decreases by 0.7%, OH decreases by 11.1%, and HO_2 decreases by 3.5% when dust is added to the atmosphere. As discussed by Ravishankara,[15] the ability for predicting accurately the composition of troposphere will depend on advances in understanding the role of particulate matter in the atmosphere and the extent to which heterogeneous reactions on solids and multiphase reactions in liquid droplets contribute to the chemistry. Thus, the heterogeneous chemistry of trace atmospheric gases on solid-phase particles in the troposphere is a field of great interest.

The primordial role of OH radicals in the oxidative transformation of volatile organic compounds and other pollutants in the troposphere has stimulated interest in the study of their atmospheric reactions. Both experimental and theoretical studies of atmospheric reactions with OH radicals in the gas phase have been reported for a large number of reactions.[16−21] In most cases, these reactions are very fast, and OH is the main oxidant of volatile organic species in the troposphere. However, the catalytic loss processes of atmospheric pollutants in the presence of OH radicals are not clear. Aerosols may promote the chemical reactions of OH radicals with adsorbed pollutants.[22,23]

Formaldehyde is an important component of the polluted troposphere, and it is a precursor of HO_x in the troposphere.

[†] Universidad Autónoma Metropolitana.
[‡] Estación Experimental del Zaidín, CSIC.
[§] CSIC-Universidad de Granada.

10.1021/jp077557m CCC: $40.75
Published on Web 02/29/2008

Thus, any heterogeneous interactions that formaldehyde may have with aerosols could potentially affect HO_x levels, especially if it is removed from the troposphere. Carlos-Cuellar et al. have recently examined the heterogeneous uptake of formaldehyde on SiO_2 using a Knudsen cell reactor.[24]

Formaldehyde may, in principle, react with an OH radical through two reaction paths: the abstraction of a hydrogen atom and the subsequent formation of a water molecule and a formyl radical; or, the addition of OH radical to the C═O double bond with the formation of the $H_2C(OH)O•$ alkoxy radical. In the gas phase at room temperature, the abstraction reaction is favored. The experimentally determined Arrhenius parameters[25,26] indicate that the activation energy barrier is negative and very small. The gas phase formaldehyde + OH reaction was studied by Alvarez-Idaboy et al.,[20] who showed that a complex mechanism, involving the formation of a prereactive complex, explains adequately the observed activation energy close to zero and the preference for the abstraction path.

One method for representing surfaces involves the use of a small cluster of atoms, often terminating unfilled valencies with hydrogen atoms or hydroxyl groups to mimic a continuous surface. The basic premise behind this approach is that reactions and adsorption are local phenomena, primarily affected by the nearby surface structure. The clusters can adopt different sizes and configurations depending on the specific system explored and the accuracy of the desired result.[27]

Theoretical studies on molecular cluster models of silicates have been performed by several authors, many of them concerning models for zeolites.[28−30] Sauer and co-workers reported an exhaustive revision of quantum mechanical models used to study molecule−solid interactions. These methods have been shown to provide useful results for local properties of solids. For example, theoretical approximations at a quantum mechanical level with cluster models have probed the correspondence between the IR experimental and calculated data for the OH vibrations in clays.[29] Molecular van der Waals complexes between adsorbed molecules and surfaces have been studied[30] and adsorption energies have been reproduced for a large number of compounds. More recently, Sauer and Sierka developed a methodology that combines quantum chemistry and interatomic potentials. They succeeded in predicting ab initio rate constants for elemental processes on the surface of solid catalysts.[31] The adsorption of methanol, formaldehyde and formic acid on Si surfaces was studied by Lu et al.[32] using DFT methods and ONIOM calculations on an Si_9H_{12} cluster model. There has been no report of a radical−molecule reaction mechanism study being performed for a molecule adsorbed on a surface.

The advantage of the cluster approach is that the active site is described explicitly by the interactions between the local molecular orbitals of adsorbate and adsorbent. This enables one to probe bonding and reactivity, and to formulate structure property relationships. On the other hand, the disadvantage is the incomplete representation of the electronic system provided by the small size and the discrete nature of the cluster employed, especially for describing the electronic band properties and for converging properly the calculations. By optimizing the adsorbate−cluster interactions carefully, the lowest energy structures and electronic states can be calculated and used to predict reliable energetic data at high levels of theory and large basis sets, thus yielding accurate energetic results. A computational study concerning the H_3SiO/CH_2O structure was carried out.[33] IR data at 170 K of the interaction of CH_2O on amorphous silica were also reported.[34] The computed harmonic vibrational frequencies were in fair agreement with those measured. For the most relevant one, the SiO−H stretching, a red shift of 129 cm^{-1} was predicted, while the observed shift was 210 cm^{-1}.

In this work, the mechanism of the formaldehyde + OH hydrogen abstraction reaction is studied, with the formaldehyde attached to a cluster model of silicate. It is clear that the results will depend significantly on the choice of the cluster model. As a first tentative approach, simple monomer, dimer, trimer and hexamer clusters are used. An exhaustive search of optimized structures for the bound formaldehyde and the stationary points on the reaction coordinate will be performed. Our aim is to identify a computational method and a cluster size and geometry that is adequate to yield reliable results for this type of reaction. To the best of our knowledge, this is the first theoretical study of a reaction between a molecule adsorbed on a silicate surface and a free radical.

Silicate Cluster Models. The rigid tetrahedron SiO_4 is the building block of all siliceous materials, from zeolites to quartz and amorphous silica. At the surface, the structures terminate either in a siloxane group with oxygen on the surface or in isolated, vicinal or geminal silanols.[35−38] These clusters can also represent both external and internal surfaces of clay minerals. The ideal surface of a phyllosilicate is characterized by the presence of a large number of siloxane Si−O−Si bridges, forming hexagonal rings. However, a natural clay surface presents many structural defects and fractures, and its chemical properties are largely due to the presence of active sites on the surface, which are mainly acid sites: Brönsted sites, associated with aluminol and silanol groups, and Lewis sites, such as in four-coordinated Al.

An isolated silanol group consists of one OH group bound to a Si atom and not interacting with other isolated sites. A geminal site has two OH groups per Si atom; because of their geometrical features, these are not mutually H-bonded. A vicinal site is made by two SiOH groups separated by one siloxane bridge; as for geminals, geometrical constraints do not allow the formation of an internal H-bond. To allow for H-bonding between SiOH groups, more than one Si−O−Si bridge is required, as is the case for interacting silanols. Thus, four different types of active sites have to be modeled by a properly chosen cluster: the siloxane bridge, isolated and geminal silanol groups, and hydroxyls in mutual interactions. Within the quantum mechanical treatment a small cluster of atoms can be used to deal with isolated irregularly distributed sites.

The easiest and chemically best defined procedure for making a cluster neutral is to saturate the dangling bonds resulting from a homolytic cut with monovalent atoms, normally hydrogen.[30] Different small clusters have been used in the literature to model silicate surfaces. Hartree−Fock (HF) results for $Si(OH)_4$ and $Si_2O(OH)_6$ are discussed by Sauer.[31] The review of Heanry et al.[39] gives a detailed account of the Si−O bond in these systems. In another review, Gibbs and Boisen[40] showed that molecular orbital calculations on molecules with first- and second-row cations (Na, Mg, Al, Si, P, S) yield bond lengths and angles that are close to those in chemically similar minerals. Recent work on chains (dimer, trimer), rings (trimer, tetramer, pentamer, hexamer), and cages (prismatic hexamer, cubic octamer, hexagonal dodecamer) was reported by Hill and Sauer[41] and Moravetski et al.[42] HF studies for the monomer, dimer, a four-silicon ring, and other silicate clusters were reported by Lasaga and Gibbs.[43,44] Recently density functional theory (DFT) work on small silicate clusters was reported.[45] Therefore, the use of these clusters has been well validated.

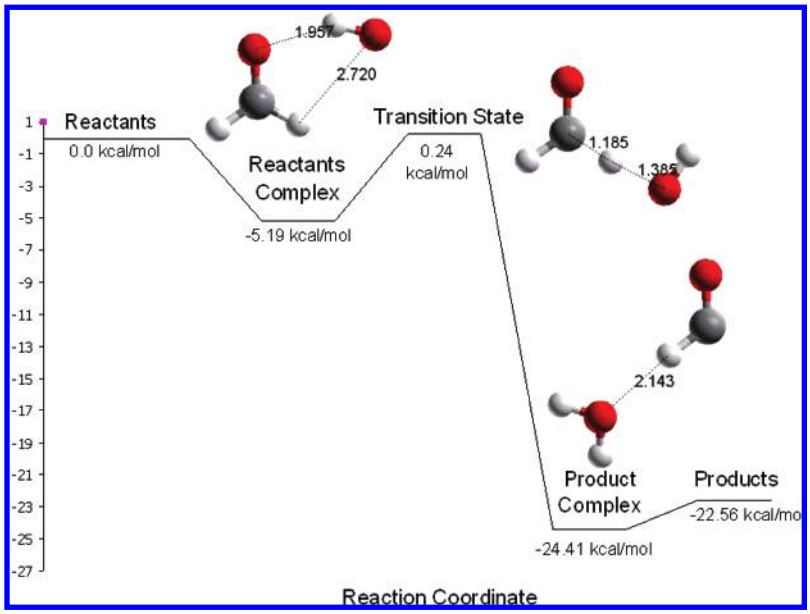

Figure 1. Gas-phase reaction energy profile. Energies are referred to the separated reactants. Atoms C, O, and H are gray, red, and white, respectively.

Surface models should represent the structural features of the system as closely as possible, while remaining limited in size. Thus, in this work, various surface models have been considered. The simplest one is the orthosilicic acid, $Si(OH)_4$ monomer, which simulates the geminal silanol groups. Vicinal silanol groups have been studied by means of the $(HO)_3Si-O-Si(OH)_3$ dimer. For isolated silanols and siloxane bridges we have used the tri-silicic acid, $(HO)_3Si-O-Si(OH)_2-O-Si(OH)_3$ trimer, in open and cyclic conformations. The hexagonal six membered ring characteristic of a clay surface has been studied by means of a cyclic hexamer model.

Computational Methodology. Ab initio quantum chemical calculations were performed using the density functional theory (DFT) method with the hybrid functional BHandHLYP/6-311G**[46,47] as implemented in the Gaussian03 program package,[48] since excellent results have been obtained with this functional in other hydrogen abstraction reactions in the gas phase.[49−51] All geometries were fully optimized at this level using the Berny analytical gradient method. No geometry constraint is applied on the surface and reactant atoms. The unrestricted approximation was used for radicals. Oftentimes, difficulties were encountered in the search for the optimized structures, with respect to convergence of the SCF. This problem was solved by using a quadratic convergence algorithm (QC), which is an option based on the Newton−Raphson method. We also employed the IOP(1/8=1) option, in order to reduce the atomic displacements, both in distances and in angles, during geometry optimization. Normal mode analyses were carried out at the same level to confirm the nature of the various stationary points, finding only positive eigenvalues for minima and one negative eigenvalue (imaginary frequency) for transition states. It was verified that the motion along the reaction coordinate corresponds to the expected transition vector. Corrections for zero-point energy (ZPE) (residual vibrational energy at 0 K) were taken from the force constant analysis and added to the total energies.

In order to study the reaction of an OH radical with a volatile organic compound adsorbed on the surface of a mineral dust aerosol model, we have chosen the reaction of a formaldehyde molecule with an OH radical. On the one hand, the formaldehyde is a very reactive polar molecule that is easily adsorbed on surfaces, and on the other hand, many theoretical and experimental data are available for the corresponding gas-phase reaction. Different cluster surfaces have been modeled. Then, formaldehyde was adsorbed on the surface, and an OH radical was allowed to approach the adsorbed formaldehyde.

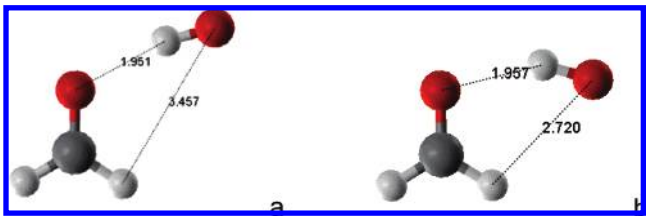

Figure 2. Molecular structure of prereactive complexes, (a) RC1 and (b) RC2, in the gas phase. Atoms C, O, and H are gray, red, and white respectively.

The gas-phase reaction of formaldehyde with an OH radical was first recalculated at the BHandHLYP/6-311G** level. Reactants, the prereactive complex (also called reactants complex), the transition state and the final intermediate product were optimized. The corresponding energy profile and structures are shown in Figure 1. In this mechanism, the reaction occurs in two steps: at first, a fast pre-equilibrium between the reactants and the prereactive complex is established, followed by an internal rearrangement leading to the elimination of a water molecule:

$$\text{step 1:}\quad RHC{=}O + OH\bullet \underset{k_{-1}}{\overset{k_1}{\rightleftharpoons}} [RHC{=}O\cdots HO\bullet] \qquad (1)$$

$$\text{step 2:}\quad [RHC{=}O\cdots HO\bullet] \xrightarrow{k_2} RC{=}O\bullet + H_2O \qquad (2)$$

Our calculated structures are similar to the ones previously found theoretically by Alvarez-Idaboy et al.[20] However, in addition to the prereactive complex obtained by these authors (RC1), another prereactive complex (RC2) was also identified (Figure 2), whose energy is 0.85 kcal/mol lower than the former. We use the new RC2 structure, where the interaction between the hydroxyl oxygen and the formaldehyde hydrogen is stronger than in RC1. Our calculated activation energy barrier is 0.24 kcal/mol, very close to the experimental results, which vary between +0.4 and −0.4 kcal/mol.[52] The product complex is also different from the one reported in ref 20. In this structure,

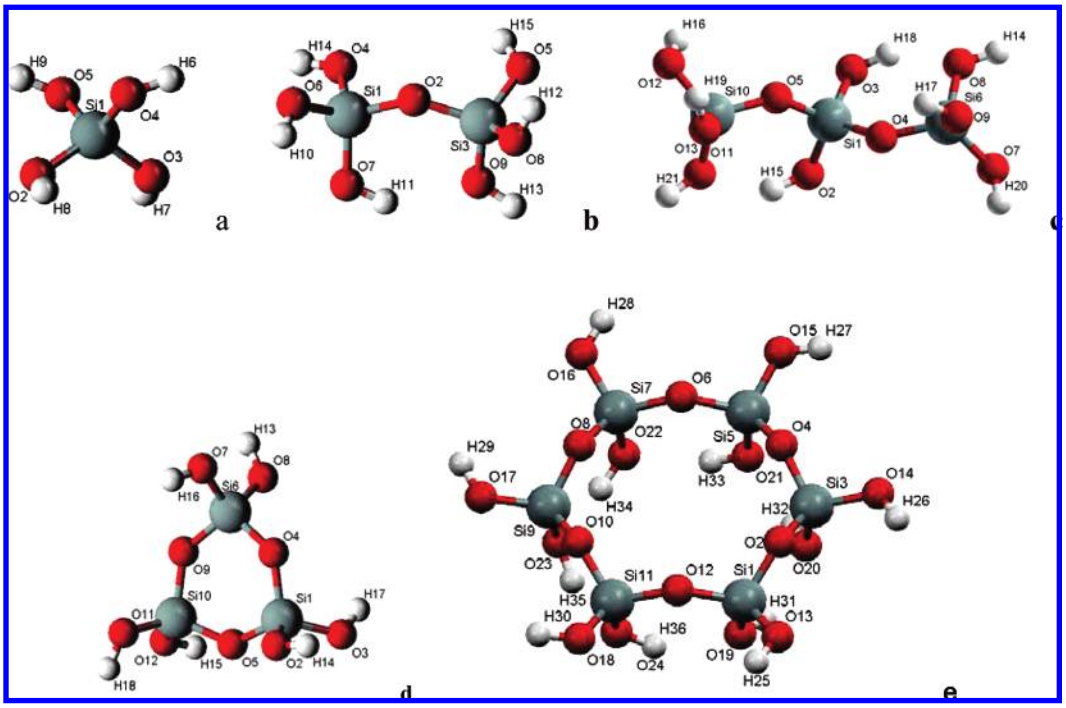

Figure 3. Molecular structure of the optimized cluster models for the mineral surface: (a) monomer, (b) dimer, (c) open trimer, (d) cyclic trimer, and (e) cyclic hexamer. Atoms Si, C, O, and H are green, gray, red, and white, respectively.

the water molecule remains attached to the formyl radical oxygen atom by a hydrogen bond (Figure 1).

The rate constant of all the studied reactions, and their Arrhenius parameters, were obtained using conventional transition state theory (CTST)[53,54] implemented in the Rate 1.1 program.[55] According to the reaction mechanism proposed above (eqs 1 and 2), if k_1 and k_{-1} are the forward and reverse rate constants for the first step and k_2 corresponds to the second step, a steady-state analysis leads to a rate coefficient for each overall reaction channel which can be written as

$$k = \frac{k_1 k_2}{k_{-1} + k_2} \tag{3}$$

Even though the energy barrier for k_{-1} is about the same size as that for k_2, the entropy change is much larger in the reverse reaction than in the formation of the products. Thus, according to a hypothesis first proposed by Singleton and Cvetanovic[56], k_2 is expected to be much smaller than k_{-1}. Based on this assumption, k can be rewritten as

$$k = \frac{k_1 k_2}{k_{-1}} = \left(\frac{A_1 A_2}{A_{-1}}\right) \exp[-(E_1 + E_2 - E_{-1})/RT] \tag{4}$$

where E_1 and E_{-1} are the step 1 energy barriers corresponding to the forward and reverse directions, respectively, E_2 is the barrier for step 2, and the A's are the partition functions. Since E_1 is zero, the net (or apparent) energy barrier for the overall reaction channel is

$$E_a = E_2 - E_{-1} = (E_{TS} - E_{RC}) - (E_{RC} - E_R) = E_{TS} - E_R \tag{5}$$

where E_{TS}, E_{RC} and E_R are the total energies of the transition state, the reactant complex and the reactants, respectively. Applying basic statistical thermodynamic principles the equilibrium constant (k_1/k_{-1}) of the fast pre-equilibrium between the reactants and the reactant complex may be obtained as where

$$K_{eq} = \frac{Q^{RC}}{Q^R} \exp\left[-\frac{E_{RC} - E_R}{RT}\right] \tag{6}$$

Q^{RC} and Q^R represent the partition functions corresponding to the reactant complex and the isolated reactants, respectively.

Under the pressure conditions in the troposphere, an equilibrium distribution of reactants is maintained in a unimolecular process and the CTST formula can be applied[57] to calculate k_2

$$k_2 = \kappa_2 \frac{k_B T}{h} \frac{Q^{TS}}{Q^{RC}} \exp\left[-\frac{E_{TS} - E_{RC}}{RT}\right] \tag{7}$$

where κ_2 is the tunneling factor, k_B and h are the Boltzmann and Planck constants, respectively, and Q^{TS} represents the transition state partition function. The energy differences include the ZPE corrections. The effective rate coefficient of each channel is then obtained as

$$k_{ef} = \sigma K_{eq} k_2 = \sigma \kappa_2 \frac{k_B T}{h} \frac{Q^{TS}}{Q^R} \exp\left[-\frac{E_{TS} - E_R}{RT}\right] \tag{8}$$

where σ is the symmetry factor, which is related to the reaction path degeneracy, and its value depends on the H atom to be abstracted. The symmetry factor is obtained by imaging all identical atoms to be labeled and by counting the number of different but equivalent arrangements that can be made by rotating (but not reflecting) the molecule.[58]

The rate constant for the gas-phase reaction obtained with the methodology used in this work agrees very well with the experimental values. Therefore, one hopes that it is possible to use the same methodology to calculate reliable kinetic data for reactions on silicate surfaces, for which experimental data are not available.

Results and Discussion

Surface Models. The optimized cluster geometries are shown in Figure 3, and the main geometrical parameters are sum-

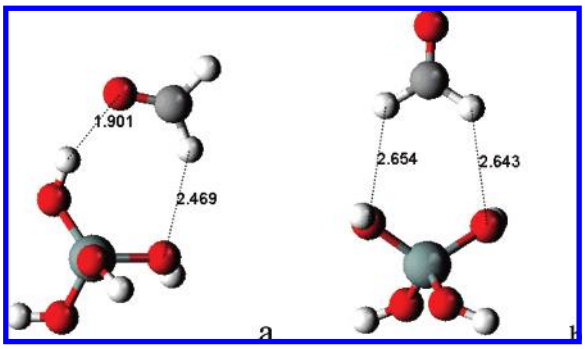

Figure 4. Adsorption of formaldehyde on the monomer surface geminal OH groups: (a) ADS1-g and (b) ADS2-g. Atoms Si, C, O, and H are green, gray, red, and white, respectively.

TABLE 1: Main Average Geometrical Features of the Optimized Surface Models and Experimental Data (Distances in Å and Angles in deg)

surface	d(Si−O)	d(O−H)	θ(OSiO)	θ(SiOSi)
monomer	1.63	0.95	106.4−115.7	
dimer	1.61−1.64	0.95	103.7−113.1	139.5
open trimer	1.62−1.64	0.95	103.9−114.8	141.1−141.6
cyclic trimer	1.62−1.64	0.95	108.2−108.6	133.2−134.4
cyclic hexamer	1.62−1.64	0.95−0.96	105.0−113.5	140.16
experiment	1.62,[a] 1.64[b]	0.95[a]		

[a] Experimental data from muscovite.[59] [b] From pyrophyllite.[60]

marized in Table 1. In all cases, full geometry optimization was achieved. The monomer has the S4 symmetry which has been experimentally determined. There is only one possible dimer, which simulates a siloxane bridge and vicinal silanol groups. For the open trimer, several minima can be found on the potential energy surface, depending on the orientation of the dihedral angles. The most stable structure was chosen. It corresponds to a linear zigzag shape trimer. Finally, two cyclic models, corresponding to the trimer and to the hexamer, were investigated.

In the optimization, all variables were named differently and allowed to vary independently. Thus, the clusters are not completely symmetric. The data reported in Table 1 are average values over similar bonds. For all surface models, the Si−O distances vary between 1.61 Å and 1.64 Å, and the O−H distances are always about 0.95 Å, both in very good agreement with experimental data for clay minerals. The O−Si−O angle varies between 103.7° and 115.7°.

Surface atomic charges are approximately constant for all cluster models. Siloxane oxygens are considerably more negative [(−0.82) − (−0.83)] than silanol oxygens [(−0.62) − (−0.70)]. The silicon atom charge increases slightly, but regularly, with the size of the cluster 1.35, 1.42, 1.43−1.51, 1.46 and 1.51 for monomer, dimer, open trimer, cyclic trimer and cyclic hexamer, respectively.

Adsorption of Formaldehyde on Surface Models. Formaldehyde adsorbs on the model surface to form an adsorption complex. It is immediately clear that a number of possibilities are available, depending on the surface characteristics. All surface−adsorbate complexes were fully optimized. In this process, the formaldehyde molecule is allowed to move freely until it reaches the optimum adsorption site. In all cases, the formaldehyde molecule lies in a plane that is perpendicular to the surface. In principle, the formaldehyde molecule can be adsorbed in two different ways: (i) When OH terminal groups are available on the surface model, the formaldehyde oxygen atom is attracted to a silanol hydrogen atom while its hydrogen atom interacts with another surface oxygen (ADS1 complexes). (ii) The formaldehyde can interact with the surface through both of its hydrogen atoms, giving rise to ADS2 adsorption complexes (Figures 4−8). In this study, we consider both adsorption pathways.

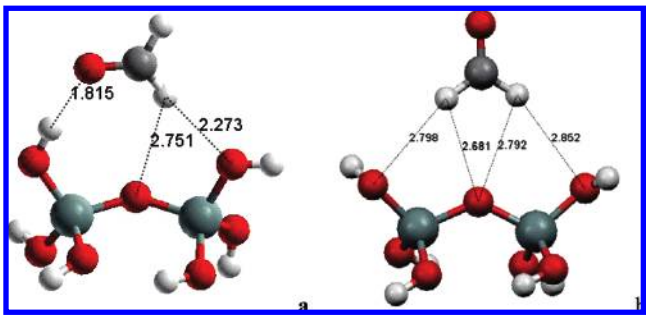

Figure 5. Adsorption of formaldehyde on the dimer surface vicinal OH groups: (a) ADS1-v and (b) ADS2-v.

In the case of the monomer, only one possible ADS1 complex is obtained (Figure 4a), with the formaldehyde oxygen and hydrogen atoms interacting with geminal OH groups (it will be called ADS1-g). For the dimer (Figure 5), which contains vicinal OH groups, a different ADS1 complex is identified, in which the formaldehyde oxygen atom is attracted mainly to one of the vicinal OH groups, while its hydrogen atom interacts with both a vicinal OH group and the siloxane bridge oxygen (it will be called ADS1-v). In the open trimer (Figure 6), which contains two siloxane bridges, the formaldehyde oxygen atom is attracted to one terminal (isolated) OH group, while its hydrogen atom is oriented toward the neighboring surface siloxane bridge. There is also a weaker interaction with the other siloxane oxygen. Thus, more interactions are present, with both siloxane bridges and terminal silanol groups (Figure 6a). This adsorption complex will be called ADS1-i. In the cyclic trimer, both ADS1-g and ADS1-v structures are obtained (Figures 7a and 7b). The former may be compared with the ADS1-g monomer complex, while the latter resembles the one for the dimer ADS1-v.

ADS2 complexes are also obtained for the monomer, the dimer, the open trimer, and the cyclic hexamer surfaces. These structures are shown in Figures 4b, 5b, 6b and 8. In the cyclic trimer, it was not possible to obtain an ADS2 structure because the formaldehyde oxygen atom tends to bind to external silanol groups rather than across the ring. In the case of the cyclic hexamer, the formaldehyde molecule lies in a plane that is perpendicular and approximately in the middle of the ring, so that its H atoms interact with the six siloxane bridges (Figure 8).

In all cases, the adsorption interactions can be considered as H-bonding. If we identify the surface atoms with a subscript s, and the formaldehyde atoms with a subscript f, in the ADS1 complexes, the $O_f\cdots H_s$ distances are about 1.81−1.90 Å, while $H_f\cdots O_s$ distances are much larger, 2.27−2.86 Å. In the ADS2 complexes, both distances between the formaldehyde hydrogens and the surface oxygens are almost the same, and they are shown in the corresponding figures. Adsorption distances in ADS2 are always larger than in ADS1, indicating weaker interactions. The geometry of the adsorbed CH_2O species is slightly different from the one of free CH_2O, i.e., the C−H and C−O bonds are slightly larger.

The adsorption energy is defined as the difference between the total electronic energy of the surface−adsorbate complex and the isolated molecule and cluster, including ZPE corrections:

$$E_{\text{adsorption}} = E_{\text{adsorption complex}} - (E_{\text{molecule}} + E_{\text{cluster}}) + \Delta(\text{ZPE}) \quad (9)$$

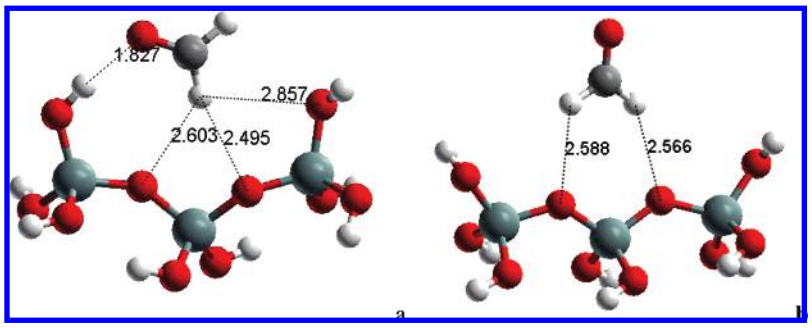

Figure 6. Adsorption of formaldehyde on a open trimer surface: (a) ADS1-i (isolated OH group) and (b) ADS2-s (siloxane bridge).

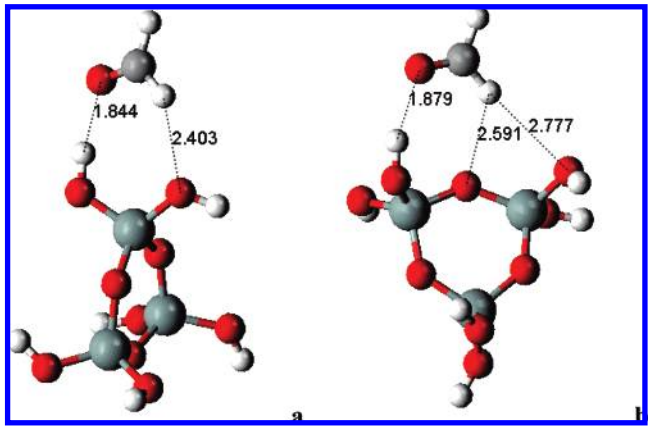

Figure 7. Adsorption complexes of formaldehyde on a cyclic trimer surface model: (a) ADS1-g and (b) ADS1-v.

The adsorption energy values, in kcal/mol, of the formaldehyde on the different surface models are summarized in Table 2. All are negative, indicating that the adsorbate is stable. ADS1 adsorption energies are more than 4 kcal/mol more negative than those of ADS2, in agreement with the shorter hydrogen bond distances. We also observe that, for the ADS1 mechanism, these values seem to be independent of the cluster size. Most models yield adsorption energies between −6.4 and −9.3 kcal/mol. Two of them present adsorption energies larger than −9 kcal/mol, due to the shape of the surface, which allows for closer interactions with terminal silanol groups. For ADS2, adsorption energy values (Table 2) increase progressively when the number of surface oxygen interactions increases: two geminal OH groups for the monomer, one siloxane bridge and two vicinal OH groups for the dimer, two siloxane bridges in the linear trimer, and six siloxane bridges in the hexamer. The net atomic charges on the siloxane bridge oxygens are more negative than the net charge on the silanol oxygen atoms. These exothermic adsorption energies indicate that these minerals are good quenchers for VOCs.

In general, the dipole moment of the ADS2 adsorption complexes is higher than that of ADS1 complexes because the formaldehyde C═O bond is highly polar and it is clearly oriented perpendicularly to the surface, while the compensation with the rest of the bonds is small (Table 2).

The adsorption energy can be plotted as a function of the distance between the formaldehyde oxygen atom and a surface hydrogen atom, $d(H_s\cdots O_f)$. An increase of adsorption energy with the decrease of this distance follows a linear relationship in the ADS1 complexes (Figure 9). However, there is no correlation between the adsorption energy and the $H_f\cdots O_s$ distance in the ADS2 complexes because, in ADS2, the interactions of the formaldehyde hydrogens with the surface oxygens are multidirectional, and also weaker than in ADS1.

Reaction between Adsorbed Formaldehyde and an OH Radical. The next step is the approach of an OH radical to the adsorbed formaldehyde molecule. It is guided mainly by the Coulomb interaction between the positively charged hydrogen atom of the OH radical and a lone pair of the formaldehyde oxygen atom. Different channels have to be considered, according to the original formaldehyde−surface adsorbate. Because ADS2 is much less bound to surface than ADS1, only channels starting from adsorption complex ADS1 type will be considered. These channels will be called M1-g, M1-v and M1-i, according to whether they start from an ADS1-g, ADS1-v or an ADS1-i adsorption complex. In this work we study five reactions: on the monomer through the M1-g channel, on the dimer by the M1-v mechanism, on the open trimer by the M1-i mechanism, and on the cyclic trimer through the M1-g and M1-v channels.

As in the gas phase, at first, a stable prereactive complex is formed, whose energy is lower than the separated reactants. In this structure, the OH radical lies in the plane of the CHO group. Then, the oxygen of OH can flip, in the plane, toward the hydrogen to be abstracted, as the energy increases to a maximum at the transition state. A product complex is then obtained that, in the next step, yields the final products.

Once the formaldehyde is adsorbed on the surface to form the ADS1 complex, the OH radical approaches it from above to remove the hydrogen atom that is not surface-bound. A free water molecule is formed, while the formyl radical remains attached to the surface. Thus the overall reaction can be written as

$$\mathbf{ADS1} + \mathrm{OH}\bullet \rightarrow \mathbf{S}\cdots\mathrm{HCO}\bullet + \mathrm{H_2O} \qquad (10)$$

where **S** stands for the surface.

Several other possibilities could be considered. In fact, depending on the orientation given to the salient water molecule, the latter could remain bound to the surface. This is especially true in the case of the linear trimer model, due to the presence of a large number of silanol groups. Thus the ΔH of the total reaction depends on the product complex formed. In this work, the mechanism will always be considered according to reaction 10.

All stationary structures for the studied surfaces are shown in Figures 10−14. Relative energy values are given in Table 3. In this table, all energies are calculated relative to the separated reactants, and include ZPE corrections: E_{-1} is the prereactive complex stabilization energy, $E_{-1} = E_{RC} - E_{reactants}$; E_2 is the reaction barrier for the second step of the complex mechanism, $E_2 = E_{TS} - E_{RC}$; E_a^{eff} is the effective activation energy, $E_a^{eff} = E_{TS} - E_{reactants}$ and ΔE is the reaction energy $\Delta E = E_{products} - E_{reactants}$. Reactions on the monomer, dimer and trimer models will be described next in detail.

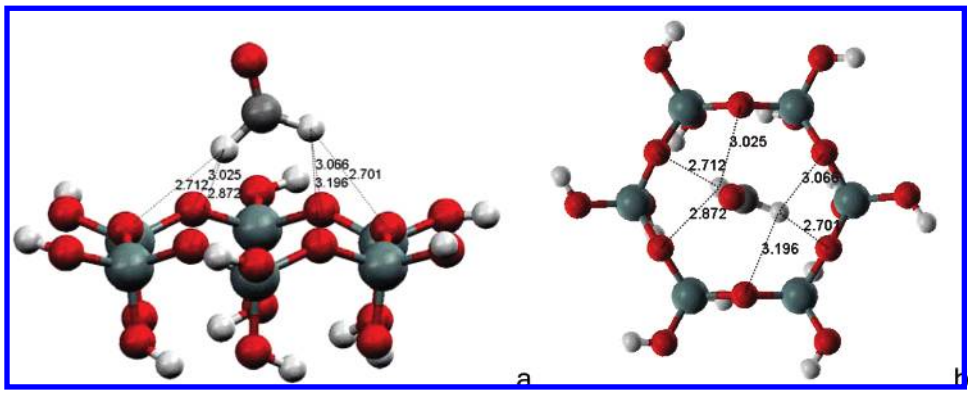

Figure 8. ADS2-s adsorption complex of formaldehyde on the cyclic hexamer surface model siloxane bridges: (a) side view and (b) top view.

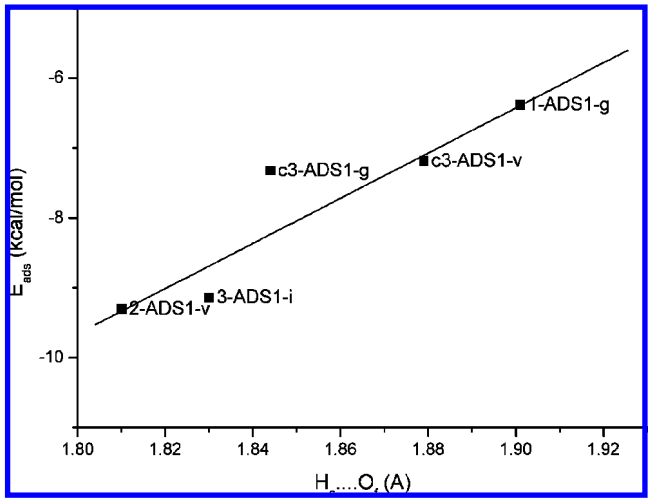

Figure 9. Adsorption energy as a function of the distance between the formaldehyde oxygen atom, O_f, and a surface (ADS1) hydrogen atom, H_s. The first number of the label accounts for the number of Si atoms of the surface model, and a "c" previous to this number stands for the cyclic trimer.

TABLE 2: Adsorption Energy (kcal/mol) and Dipole Moment (debyes) for the Adsorption Complexes (s Means Siloxane Bridge Oxygen)

surface	adsorption sites	adsorption complex	$E_{adsorption}$	dipole moment
monomer	OH−OH	ADS1-g	−6.38	2.93
dimer	OH−s−OH	ADS1-v	−9.30	1.09
open trimer	OH−s−s−OH	ADS1-i	−9.14	4.17
cyclic trimer	OH−OH	ADS1-g	−7.32	2.36
cyclic trimer	OH−s−OH	ADS1-v	−7.18	3.08
monomer	geminal OH	ADS2-g	−1.99	3.85
dimer	vicinal OH	ADS2-v	−2.67	4.48
open trimer	1 siloxane bridge	ADS2-i	−3.43	3.13
cyclic hexamer	ring siloxane bridges	ADS2-s	−3.67	3.63

Prereactive Complexes. The OH radical attack channel is the same in all adsorption models. In the prereactive complexes, the OH radical hydrogen atom approaches the oxygen of the formaldehyde. The interactions determine the shape and stability of the prereactive complexes as well as the rest of the reaction. The structure of the adsorption complex remains almost unchanged in this process. The prereactive complexes are shown in Figures 10a, 11a, 12a, 13a and 14a, and the nonbonding O···H distances between the OH radical and the adsorbed formaldehyde are given in Table 3. Atoms belonging to the OH radical are indicated with the oh subscript, while those from formaldehyde carry the f subscript.

As in the gas phase, we note that the most important interaction is the one between the OH hydrogen atom and the formaldehyde O atom. The $H_{oh}\cdots O_f$ distance is always considerably smaller than $d(O_{oh}\cdots H_f)$. While the former distance is quite constant and about 1.96−1.99 Å, the latter ranges from 2.668 to 3.331 Å. These values are close to those in the gas phase, indicating a similar geometry for all the prereactive complexes. Nevertheless, the $d(O_{oh}\cdots H_f)$ value in the gas-phase complex is similar to the one in the monomer and slightly smaller than for the rest of the complexes. For the cyclic trimer, there are two possible prereactive complexes, corresponding to the adsorption complexes ADS1-g and ADS1-v. Nonbonding O···H distances are similar in both, which means that the geometry of the prereactive complex is approximately independent of the formaldehyde orientation on the surface.

As can be seen in Table 3, all prereactive complexes are stable, with E_{-1} stabilization energies lying between −3.72 and −4.15 kcal/mol. All are less stable than in the gas phase. This could indicate that, when the reaction occurs on a silicate surface near terminal silanol groups, the reverse reaction will be more feasible than in gas phase.

Transition States. In all cases, transition states resemble the one in the gas-phase reaction, because the hydrogen atom that is to be abstracted is free of surface interactions. Inspection of the vibrational mode corresponding to the imaginary frequency of the transition states indicates that this vibration is essentially the motion of a light atom (H) between two fixed heavier atoms (C and O). There is little heavy atom motion as the system moves along the reaction path. The negative frequencies corresponding to the motion along the reaction path have also been indicated for the transition states in Table 3. All are close to 1200 cm^{-1} and larger than in the gas phase, except for the open trimer. Indeed, for the open trimer, the geometry of the transition state is different from the other cases considered, because the OH radical has the possibility to interact with terminal silanol groups, yielding an unusually stable transition state (Figure 12b). The corresponding transition vector, however, shows the characteristic H atom motion between the C_f and O_{oh} atoms.

The shape of the M1-g TS structure of the cyclic trimer resembles the M1-g monomer TS, although all the relevant interacting distances are slightly shorter in the former. Analogously, the shape of the M1-v TS in the cyclic trimer is close to the M1-v dimer TS. It is interesting to note that in the case of the cyclic trimer, the relative energies are very similar for both M1-v and M1-g channels (Table 3), indicating that they are almost independent of the ADS1 adsorption complex shape.

In the monomer, the energy barrier of the second step, E_2, is slightly larger than in gas phase (Table 3). For all the other models E_2 is smaller than in gas phase, especially for the open trimer that has the lowest E_2 value. However, two very different

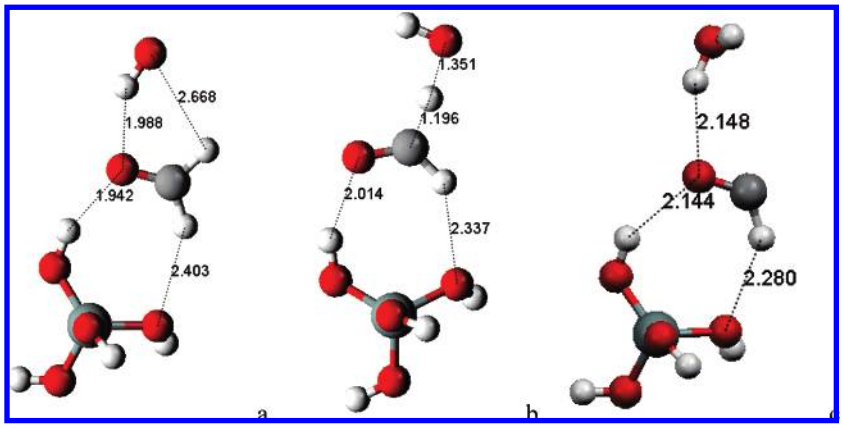

Figure 10. Reaction on the monomer surface (M1-g): (a) prereactive Complex (RC), (b) transition state (TS), and (c) product complex (PC).

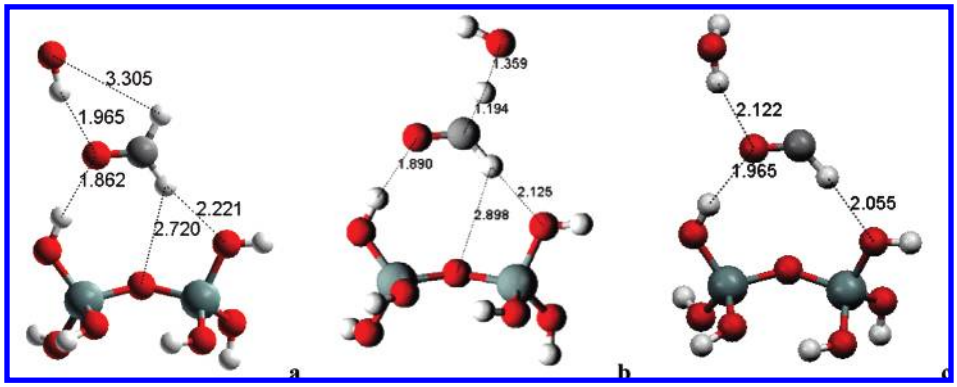

Figure 11. Reaction on the dimer surface (M1-v): (a) prereactive Complex (RC), (b) transition state (TS), and (c) product complex (PC).

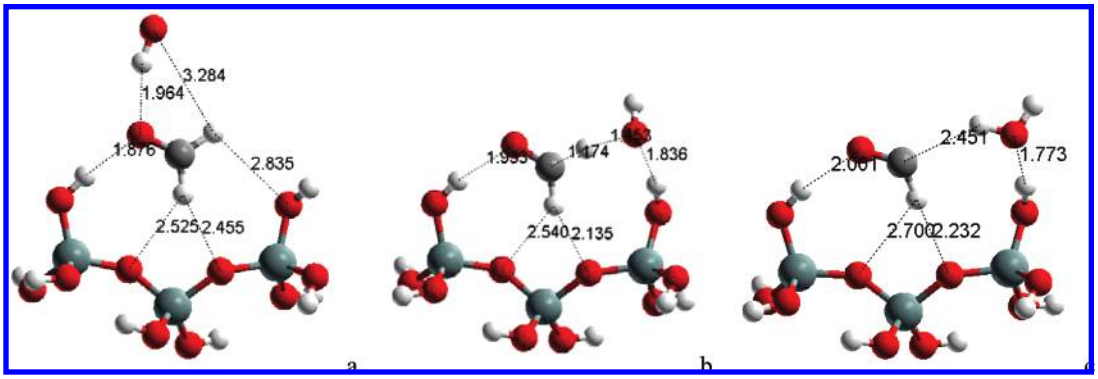

Figure 12. Reaction on the open trimer surface (M1-i): (a) prereactive complex (RC), (b) transition state (TS), and (c) product complex (PC).

situations occur that are not related to the size of the cluster. When no additional silanol groups are present close to the reaction site, the transition state is similar to the one in the gas phase, and the formed water molecule separates from the surface, while the formyl radical remains adsorbed. This is the case for the monomer, dimer and cyclic trimer. For all of them the energy barrier E_2 is about 4.8 kcal/mol and lower than in the gas phase (5.43 kcal/mol). However, it is important to note that the effective activation energies are always about 1 kcal/mol, and larger than in the gas phase. This effect, of course, is mainly due to the higher energy of the prereactive complex. It suggests that the presence of the silicate surface does not favor significantly this reaction. We shall see later that the rate constants results agree with this conclusion.

In the other case, when silanol groups are available close to the reaction site, the transition state occurs very close to the surface, interacting with another one of these silanol groups. This is the case of the open trimer model, both the water molecule and the formyl radical remain attached to the surface, leading to a low-energy barrier E_2 (1.39 kcal/mol). The corresponding E_a^{eff} is very negative (−2.76 kcal/mol), and considerably lower than in the gas phase (0.24 kcal/mol). This model is completely different from the others. The open trimer may be a valid model for situations where many silanol groups are available on the surface, but we find that the OH reaction with formaldehyde attached to the open trimer has a potential energy surface that presents several close minima, both for the surface and for the stationary points along the reaction path. Therefore, reliable conclusions for such small energy differences as those involved in the present calculations cannot be obtained for this last model. Further calculations will be performed exploring the relevance of additional models and the ADS2 complexes.

A plot of the E_2 barrier as a function of the adsorption energy is shown in Figure 15. The adsorption energy of the gas-phase reaction has been set equal to zero. It can be seen that, when

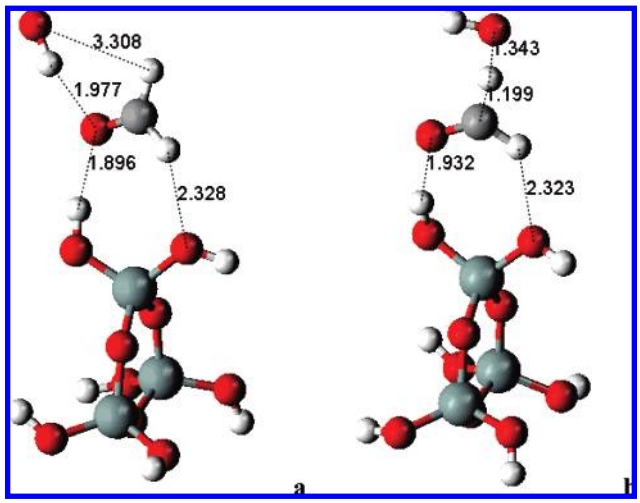

Figure 13. Reaction on the cyclic trimer surface (M1-g): (a) prereactive complex (RC) and (b) transition state (TS).

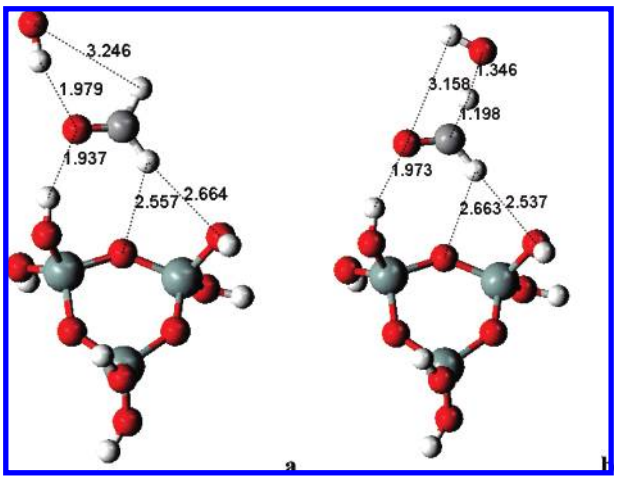

Figure 14. Reaction on the cyclic trimer surface (M1-v): (a) prereactive complex (RC) and (b) transition state (TS).

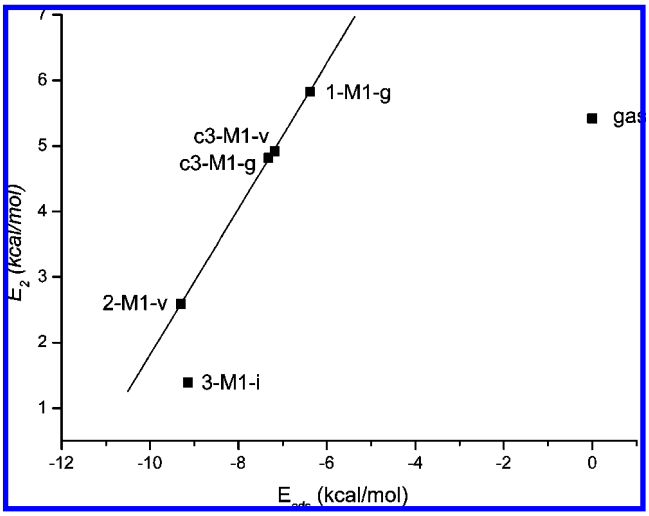

Figure 15. Energy barrier E_2 as a function of adsorption energy. The first number of the label accounts for the number of Si atoms of the surface model, and a "c" previous to this number stands for the cyclic trimer.

the adsorption energy increases, the corresponding E_2 barrier decreases. This very clear correlation signals the influence of the presence of the silicate surface on the reaction barrier E_2.

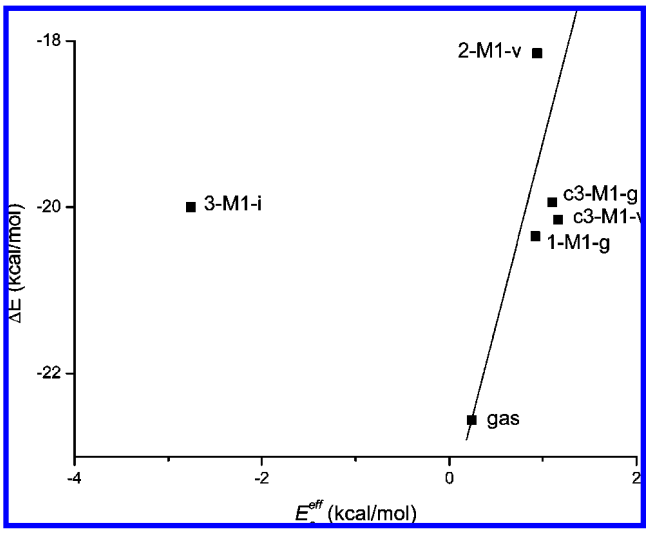

Figure 16. Reaction energy as a function of the effective activation energy. The first number of the label accounts for the number of Si atoms of the surface model, and a "c" previous to this number stands for the cyclic trimer.

As discussed above, the open trimer does not fit well in the correlation due to its peculiar geometry and to its low E_2 energy barrier.

Products. In this work, the reaction energies are calculated according to reaction 4 (Table 3). In Figure 16 we plot ΔE against the effective activation energy. We can appreciate an approximately linear correlation, not including the M1-i of the linear trimer (3-M1-i) that presents different interactions as discussed above. In the product structure for 3-M1-i, the water molecule is physiadsorbed on a silanol of the cluster model. In the other reactions the water molecule formed is free from the cluster interaction. Therefore, both mechanisms, M1 and the gas-phase reaction, fall on the same linear correlation.

The geometry and relative energy of the product complexes appear to be approximately independent of the cluster size, except in the open trimer where the water molecule is anchored to the surface. Reaction energies are always about −20 kcal/mol, smaller than in the gas phase.

Reaction Rate Constants. The rate constants for all the studied reactions have been determined as a function of temperature using transition state theory. In all cases the complex mechanism, eqs 1 and 2, has been assumed to occur. The energy values, partition functions and thermodynamic data were taken from the quantum chemistry calculations. The effective rate constant is obtained using the following equation:

$$k_{ef} = \sigma\kappa_2 \frac{Q^{TS}}{Q^R} \exp\left[-\frac{E_a^{eff}}{RT}\right] \qquad (11)$$

The tunneling correction κ_2 of the second step is calculated according to the Eckart[61] model. It depends on the size and shape of the E_2 barrier. Except in the open trimer, for which the E_2 barrier is much smaller, κ_2 is approximately constant and lies between 4 and 5. The Arrhenius parameters are obtained from the rate constants (in cm^3 $molecule^{-1}$ s^{-1}), plotting the logarithm of rate constants vs $1000/T$ in the range 273 to 318 K (Table 4).

In agreement with the fact that the effective activation energies are larger than in the gas phase for most cases, the calculated rate constants are smaller than in the gas phase. For the monomer, dimer and cyclic trimer, the rate constant is approximately 1 order of magnitude smaller than in the gas

TABLE 3: Relative Energies (Including ZPE) in kcal/mol, Imaginary Frequencies (Im Freq) at the Transition States (in cm^{-1}), and Nonbonding O···H Distances (in Å) in the Prereactive Complexes for the OH Radical Reaction with Formaldehyde on the Surface Models and in the Gas Phase

surface	reaction	E_{ads}	E_{-1}	E_2	E_a^{eff}	ΔE	Im Freq	$H_{oh}\cdots O_f$	$O_{oh}\cdots H_f$
monomer	M1-g	−6.37	−3.85	4.76	0.90	−20.37	−1,204	1.99	2.67
dimer	M1-v	−9.30	−3.91	4.85	0.94	−18.15	−1,148	1.96	3.30
open trimer	M1-i	−9.14	−4.15	1.39	−2.76	−20.00	−659	1.96	3.28
cyclic trimer	M1-g	−7.32	−3.72	4.82	1.10	−19.94	−1,271	1.98	3.31
cyclic trimer	M1-v	−7.19	−3.76	4.92	1.16	−20.15	−1,260	1.98	3.25
	gas phase		−5.19	5.43	0.24	−22.56	−932	1.96	2.72

TABLE 4: Rate Constants (in cm^3 $molecule^{-1}$ s^{-1}) and Arrhenius Parameters at 298 K for All the Studied Reactions (Experimental Values in Parentheses)

reaction	σ	K_{eq} (cgs)	κ_2	k_2 (s^{-1})	A	Ea/R	k_{ef}
gas phase	2	1.38×10^{-21}	2.64	7.78×10^{9}	4.62×10^{15}	3.96×10^{3}	1.07×10^{-11} (1.0×10^{-11})
monomer	1	4.72×10^{-22}	4.45	3.67×10^{9}	4.59×10^{15}	4.18×10^{3}	1.73×10^{-12}
dimer	1	3.97×10^{-22}	4.00	2.72×10^{9}	3.52×10^{15}	4.19×10^{3}	1.08×10^{-12}
open trimer	1	2.29×10^{-21}	1.63	1.88×10^{9}	3.56×10^{11}	1.56×10^{3}	4.31×10^{-12}
cyclic trimer M1 g	1	1.78×10^{-22}	5.13	7.83×10^{9}	1.16×10^{16}	4.24×10^{3}	1.39×10^{-12}
cyclic trimer M1v	1	3.30×10^{-22}	5.07	2.78×10^{9}	4.43×10^{15}	4.26×10^{3}	0.92×10^{-12}

phase. In the case of the open trimer, the rate constant is about half this value, as expected from the additional stability of the transition state, in which the OH radical is very close to a surface silanol group. The value of the *A* factor, however, is also much smaller than in the other transition states, due to the particular tightness of the TS, thus compensating for the large difference in the exponential. It is important to mention that, in all cases, the reaction symmetry number is equal to one, because only one H atom from formaldehyde can be abstracted. In the gas phase, this number is equal to two.

Conclusions

In this work, the mechanism of the reaction between an OH radical and a formaldehyde molecule attached to a silicate cluster model is studied with the BHandHLYP/6-311G** quantum chemistry method. Several surface models are used to mimic a natural silicate surface: a monomer, a dimer, a linear and cyclic trimer, and an hexamer. The adsorption of formaldehyde is studied on all model surfaces and in different relative orientations, considering that formaldehyde may interact with surface atoms either using its oxygen and one hydrogen atom, or through both hydrogen atoms (called ADS1 and ADS2 adsorption types, respectively). The case of the cyclic hexamer is included because it is representative of an adsorption through the interaction of both hydrogen atoms of formaldehyde with the oxygen atoms of siloxane bridges (ADS2 adsorption type).

The potential energy surfaces for the formaldehyde interaction with the surface models are carefully spanned, and minima and maxima are evaluated. We find that, when silanol groups are available, the adsorption always occurs preferentially on them, forming ADS1-type complexes. Interaction with the siloxane bridges is much less favorable, and adsorption complexes that only use siloxane bridges (called ADS2 in this work) have adsorption energies at least 4 kcal/mol less negative than the ADS1 ones. This is the case, for example, of the cyclic hexamer where the formaldehyde molecule is adsorbed in the middle of the ring with its H atoms interacting with all six siloxane bridges. Since natural silicates present numerous fractures and, in general, silanol groups are available, one can expect that adsorption of formaldehyde will normally occur in their vicinity and form ADS1-type complexes. In all cases, when silanol groups are present, the adsorption energy is between 7 and 9 kcal/mol. Thus, adsorption on the terminal silanol groups seems to be a local effect, and increasing the cluster size is not expected to yield more accurate calculated results. The significant negative adsorption energy reveals that the surface model is a good quencher for VOCs, with interesting implications in atmosphere.

The ADS2 adsorption-type is found to yield considerably less stable complexes and to be less probable than the ADS1 ones, hence the reaction with the OH radical is studied only for ADS1 complexes.

As in the gas phase, in the surface models the OH radical reacts with formaldehyde to form a water molecule and a formyl radical. The latter remains attached to the surface.

It is very interesting to note that, in all cases, regardless of the adsorption energies, the effective activation energies E_a^{eff} are always about 1 kcal/mol, and larger than in the gas phase, suggesting that the presence of silicates does not favor the reaction. This is in agreement with the kinetic results that indicate that the rate constants are smaller than in the gas phase by about 1 order of magnitude. This is only partially due to the change in the symmetry number that goes from 2 in the gas phase to 1 in the presence of the surface.

The open trimer model does not fit into the observed tendencies for the monomer, dimer and cyclic trimer. The possibility to assume a large number of conformations with similar energies allows it to bind to both reactants in many ways and to yield a transition state with a much lower barrier than for the other models. Yet, even this model yields a reaction rate constant that is smaller than the gas-phase constant. This result lends additional support to our conclusion that the presence of a silicate in the troposphere does not catalyze the reaction between formaldehyde and OH free radicals. If one takes into account the fact that, in addition, silicate aerosols trap VOCs and OH radicals in the troposphere, the resulting decrease in the formaldehyde reaction rate with OH can be significant.

Acknowledgment. Authors are thankful to the Mexican agency CONACYT through Grant SEP-2004-C01-46167 and to PIFI 3.3 for the acquisition of computer clusters on which calculations were performed. This work was also supported by an international cooperation project CSIC-CONACYT (ref 2004MX0017) and the Spanish MCYT and European FEDER Grants BTE2002-03838, and CTQ2004-04648.

References and Notes

(1) Tegen, I.; Fung, I. *J. Geophys. Res.* **1994**, *99*, 22897.
(2) Prospero, J. M. *Proc. Natl. Acad. Sci. U.S.A.* **1999**, *96*, 3396.

(3) Prospero, J. M. In *The Impact of Desert Dust Across the Mediterranean*; Guerzoni, S., Chester, R., Eds.; Kluwer: Dordrecht, The Netherlands, 1996.
(4) Duce, R. A. In *Aerosol Forcing of Climate*; Charlson, R. J., Heintzenberg, J., Eds.; Wiley: Chichester, U.K., 1995.
(5) Andreae, M. O. In *World Survey of Climatology*'s *Future Climates of the World: A Modelling Perspective*; Henderson-Sellers, A., Ed.; Elsevier: Amsterdam, The Netherlands, 1995; Vol. 16.
(6) Prospero, J. M.; Olmez, I.; Ames, M. *Water, Air, Soil Pollut.* **2001**, *125*, 291.
(7) Perry, K. D.; Cahill, T. A.; Eldred, R. A.; Dutcher, D. D.; Gill, T. E. *J. Geophys. Res.* **1997**, *102*, 11225.
(8) Coude-Gaussen, G.; Rogon, P.; Bergametti, G.; Gomes, L.; Strauss, B.; Gros, J. M.; Coustumer, M. N. *J. Geophys. Res.* **1987**, *D8*, 9753.
(9) Chester, R. *Sci. Geol. Mem.* **1990**, *88*, 23.
(10) Gomes, L.; Gillette, D. A. *Atmos. Environ.* **1993**, *27A*, 2539.
(11) Miller, R. L.; Tegen, I.; Perlwitz J. *J. Geophys. Res.* **2004**, *109*, D04203.
(12) Usher, C. R.; Michel, A. E.; Grassian, V. H. *Chem. Rev.* **2003**, *103*, 4883.
(13) Dentener, F. J.; Carmichael G. R.; Zhang Y. *J. Geophys. Res*. **1996**, *101*, 22869.
(14) Bian, H. S.; Zender, C. S. *J. Geophys. Res.* **2003**, *108*, 4672.
(15) Ravishankara, A. R. *Science* **1997**, *276*, 1058.
(16) Atkinson, R. *Atm. Environ.* **2000**, *34*, 2063.
(17) Atkinson, R.; Baulch, D. L.; Cox, R. A.; Hampson, R. F.; Kerr, J. A.; Rossi, M. J.; Troe, J. *J. Phys. Chem. Ref. Data* **1999**, *28*, 191.
(18) Baulch, D. L.; Cox, R. A.; Hampson, R. F.; Kerr, J. A.; Rossi, M. J.; Troe, J. *J. Phys. Chem. Ref. Data* **2000**, *29*, 167.
(19) Uc, V. H.; Grand, A.; Vivier-Bunge, A. *J. Mol. Struct. (THEOCHEM)* **2004**, *684*, 171.
(20) Alvarez-Idaboy, J. R.; Mora-Diez, N.; Boyd, R.; Vivier-Bunge, A. *J. Am. Chem. Soc*. **2001**, *123*, 2018.
(21) Alvarez-Idaboy, J. R.; Mora-Díez, N.; Vivier-Bunge, A. *J. Am. Chem. Soc*. **2000**, *122*, 3715.
(22) Oh, S.; Andino, J. M. *Atm. Environ.* **2002**, *36*, 149.
(23) Sørensen, M.; Hurley, M. D.; Wallington, T. J.; Dibble, T. S.; Nielsen, O. J. *Atm. Environ*. **2002**, *36*, 5947.
(24) Carlos-Cuellar, S.; Li, P.; Christensen, A. P.; Krueger, B. J.; Burrichter, C.; Grassian, V. H. *J. Phys. Chem. A* **2003**, *107*, 4250.
(25) Atkinson, R.; Baulch, D. L.; Cox, R. A.; Hampson, R. F., Jr.; Kerr, J. A.; Rossi, M. J.; Troe, J. *J. Phys. Chem. Ref. Data* **1997**, *26*, 521.
(26) DeMore, W. B.; Sander, S. P.; Golden, D. M.; Hampson, R. F.; Kurylo, M. J.; Howard, C. J.; Ravishankara, A. R.; Kolb, C. E.; Molina, M. J., JPL-PUBL-92−20; NAS 1.26192795; NASA-CR-192795.
(27) Apai, G.; Hamilton, J. F.; Stohr, J.; Thompson, A. *Phys. Rev. Lett.* **1979**, *43*, 165.
(28) Lasaga, A. C. Fundamental approaches in describing mineral dissolution and precipitation rates. In *Chemical Weathering rates of silicate minerals*; White, A. F., Brantley, S. L., Eds.; Reviews in Mineralogy, Vol. 31; Mineralogical Society of America: Washington, DC, 1995; pp 23−86.
(29) Sainz-Díaz, C. I.; Timón, V.; Botella, V.; Hernández-Laguna, A. *Am. Mineral.* **2000**, *85*, 1038.
(30) Sauer, J.; Ugliengo, P.; Garrone, E.; Saunders, V. R. *Chem. Rev.* **1994**, *94*, 2095.
(31) Sauer, J. *Chem. Rev.* **1989**, *89*, 199.
(32) Lu, X.; Zhang, Q.; Lin, M. C. *Phys. Chem. Chem. Phys.* **2001**, *3*, 2156.
(33) Ugliengo, P.; Saunders, V. R.; Garrone, E. *Chem. Phys. Lett.* **1990**, *169*, 501.
(34) Busca, G.; Lamotte, J.; Lavalley, J. C.; Lorenzelli, V. *J. Am. Chem. Soc*. **1987**, *109*, 5197.
(35) Van Roosmalen, A. J.; Mol, J. C. *J. Phys. Chem.* **1978**, *82*, 2748.
(36) Burneau, A.; Barrés, O.; Gallas, J. P.; Lavalley, J. C. *Langmuir* **1990**, *6*, 1364.
(37) Bronnimann, C. E.; Zeigler. R. C.; Maciel, G. E. *J. Am. Chem. Soc.* **1988**, *110*, 2023.
(38) Léonardelli, S.; Facchini, L.; Fretigny, C.; Tougne, P.; Legrand, A. P. *J. Am. Chem. Soc.* **1992**, *114*, 6412.
(39) Heanry, P. J.; Prewitt, C. T.; Gibbs, G. V. In *Silica, Physical Behavior, Geochemistry and Materials Applications*; Ribbe, P. H., Ed.; Reviews in Mineralogy, Vol. 29; Mineralogical Society of America: Washington, D.C., 1994; p 331.
(40) Gibbs, G. V.; Boisen, M. B. In *Better Ceramics Through Chemistry II*; Brinker, C. J., Clark, D. E., Ulrich, D. R., Eds.; Materials Research Society, Vol. 73; Elsevier Science Publishing Co., Inc.: New York, 1986; p 515.
(41) Hill, J.; Sauer, J. *J. Phys. Chem.* **1994**, *98*, 1238.
(42) Moravetski, V.; Hill, J.; Eichler, U.; Cheetham, A. K.; Sauer, J. *J. Am. Chem. Soc.* **1996**, *118*, 13015.
(43) Lasaga, A. C.; Gibbs, G. V. *Phys. Chem. Miner*. **1987**, *14*, 107.
(44) Lasaga, A. C.; Gibbs, G. V. *Am. J. Sci.* **1990**, *290*, 263.
(45) Pápai, I.; Goursot, A.; Fajula, F. *J. Phys. Chem.* **1994**, *98*, 4654.
(46) Becke, A. D. *J. Chem. Phys.* **1993**, *98*, 1372.
(47) Raghavachari, K.; Foresman, J. B.; Cioslowski, J.; Ortiz, J. V.; Frisch, M. J.; Frisch, A. *GAUSSIAN 98 User's Reference*; Gaussian Inc.: Pittsburgh, PA, 1998.
(48) Frisch, M. J.; Trucks, G. W.; Schlegel, H. B.; Scuseria, G. E.; Robb, M. A.; Chesseman, J. R.; Zarzewki, V. G.; Montgomery, J. A.; Stratmann, R. E.; Burant, J. C.; Dapprich, S.; Millam, J. M.; Daniels, A. D.; Kudin, K. N.; Strain, M. C.; Farkas, O.; Tomasi, J.; Barone, V.; Cossi, M.; Cammi, R.; Mennucci, B.; Pomelli, C.; Adamo, C.; Clifford, S.; Ochterski, J.; Petersson, G. A.; Ayala, P. Y.; Cui, Q.; Morokuma, K.; Malick, D. K.; Rabuck, A. D.; Raghavachari, K.; Foresman, J. B.; Cioslowski, J.; Ortiz, J. V.; Stefanov, B. B.; Liu, G.; Liashenko, A.; Piskorz, P.; Komaromi, I.; Gomperts, R.; Martin, R. L.; Fox, D. J.; Keith, T. A.; Al-Laham, M. A.; Peng, C. Y.; Nanayakkara, A.; Gonzalez, C.; Challacombe, M.; Gill, P. M. W.; Johnson, B. G.; Chen, W.; Wong, M. W.; Andres, J. L.; Head-Gordon, M.; Replogle, E. S.; Pople, J. A. *Gaussian 03*, revision A.1; Gaussian, Inc.: Pittsburgh, PA, 2004.
(49) Galano, A.; Alvarez-Idaboy, J. R.; Ruiz-Santoyo, M. E.; Vivier-Bunge, A. *J. Phys. Chem. A* **2005**, *109*, 169.
(50) Galano, A.; Alvarez-Idaboy, J. R.; Ruiz-Santoyo, M. E.; Vivier-Bunge, A. *J. Phys. Chem. A* **2002**, *106*, 9520.
(51) Galano, A.; Alvarez-Idaboy, J. R.; Bravo-Pérez, G.; Ruiz-Santoyo, M. E. *Phys. Chem. Chem. Phys.* **2002**, *4*, 4648.
(52) The NIST Chemical Kinetics Data Base, NIST Standard Reference Database; U.S. Dept. of Commerce, Technology Administration, National Institute of Standards and Technology: Gaithersburg, MD, 17-2Q98.
(53) Eyring, H. *J. Chem. Phys.* **1935**, *3*, 107.
(54) Truhlar, D. G.; Hase, W. L.; Hynes, J. T. *J. Phys. Chem.* **1983**, *87*, 2264.
(55) Duncan, W. T.; Bell R. L.; Truong, T. N. *J. Comput. Chem.* **1998**, *19*, 1039.
(56) Singleton, D. L.; Cvetanovic, R. J. *J. Am. Chem. Soc*. **1976**, *98*, 6812.
(57) Pilling, M. J.; Seakins, P. W. *Reaction Kinetics*; Oxford University Press: New York, 1996.
(58) Laidler, K. J. *Chemical Kinetics*; Harper Collins Publishers: New York, 1987; p 98.
(59) Guggenheim, S.; Chang, Y.-H.; Koster van Gross, A. F. *Am. Mineral.* **1987**, *72*, 537.
(60) Lee, J. H.; Guggenheim, S. *Am. Mineral.* **1981**, *66*, 350.
(61) Truong, T. N.; Truhlar, D. G. *J. Chem. Phys.* **1990**, *93*, 1761.